This manuscript has been published in Microscopy and Microanalysis, 2015 Oct 16:1-19.

PubMed PMID: 26471836.

Title: Improved sealing and remineralization at the resin-dentin interface after phosphoric acid etching and load cycling.

Running title: Remineralization of dentin after acid etching and load cycling.

Authors: Manuel Toledano[1*], Inmaculada Cabello[1], Fátima S. Aguilera[1], Estrella Osorio[1], Manuel Toledano-Osorio[1], Raquel Osorio[1].

Institution: [1]University of Granada, Faculty of Dentistry, Dental Materials Section.

Address: [1]University of Granada, Faculty of Dentistry, Dental Materials Section
Colegio Máximo de Cartuja s/n
18071 – Granada - Spain.

*Corresponding author: Prof. Manuel Toledano
University of Granada, Faculty of Dentistry
Dental Materials Section
Colegio Máximo de Cartuja s/n
18071 – Granada - Spain.
Tel.: +34-958243788
Fax: +34-958240809
Email: toledano@ugr.es

ABSTRACT

Introduction. The purpose of this study was to investigate the micro-morphology of the resin-dentin inter-diffusion zone using two different single-bottle self-etching dentin adhesives with and without previous acid-etching, after *in vitro* mechanical loading stimuli. *Materials and Methods*. Extracted human third molars were sectioned to obtain dentin surfaces. Two different single-bottle self-etching dentin adhesives, Futurabond U (FUT) and Experimental (EXP) both from VOCO, were applied following the manufacturer's instructions or after 37% phosphoric acid application. Resin-dentin interfaces were analyzed with dye assisted confocal microscopy evaluation (CLSM), including the calcium-chelation technique, xylenol orange (CLSM-XO). *Results.* The confocal microscopy revealed that resin-dentin interfaces of unloaded specimens were deficiently resin-hybridized, in general. These samples showed a rodhamine B-labeled hybrid complex and adhesive layer completely affected by fluorescein penetration (nanoleakage) through the porous resin-dentin interface, but thicker after phosphoric acid-etching. Load cycling promoted an improved sealing of the resin-dentin interface at dentin, a decrease of the hybrid complex porosity, and an increment of dentin mineralization. Load cycled specimens treated with the xylenol orange technique produced a clearly outlined fluorescence due to a consistent Ca-mineral deposits within the bonding interface and inside the dentinal tubules, especially when the experimental adhesive was applied.

Key words: dentin, load cycling, fluoresceine, rodhamine, xylenol orange, confocal microscopy

INTRODUCTION

Aesthetic resin-based dental materials are commonly employed for dental restorations due to their tooth-like appearance. Self-etching adhesives are based on the use of polymerizable acidic monomers that simultaneously condition/prime, to a depth <1 μm (mild self-etching adhesives) (De Munck et al., 2010), and bond dentin. The self-etching systems were introduced to eliminate the conditioning, rinsing and drying steps, which are technique sensitive and difficult to standardize under clinical conditions (Tay et al., 1996). Even when the self-etching approach seems to reduce the non-resin covered collagen layer, this unprotected collagen may become the sites for collagen hydrolysis by host-derived matrix metalloproteinase (MMP) enzymes (Toledano et al., 2012). The clinical success of resin adhesion to dentin is, therefore, undermined because of the loss of integrity at the resin-dentin interface (Spencer et al., 2010). Thus, the bonded interface at the dentin remains the Achilles' heel of dental restorations (Oguri et al., 2012).

Diffusion of acidic resin monomers through the smear layer is slow (Nakabayashi & Saimi, 1996), and once reinforced by impregnated resin, the final bonding efficacy may be too low to provide strong, durable mechanical properties. The mineralized components of the smear layer are efficient buffers, making the pH of acidic monomers too high to demineralize the underlying dentin, and the presence of thick smear layers may interfere with the diffusion of self-etching primers into the intact underlying dentin. Therefore, more stable bonds may be formed if primers and resins are able to penetrate through the smear layer and interact with the underlying dentin. Additionally, such demineralization is promoted by components which are less acidic than 35% phosphoric acid used in etch&rinse bonding agents, originating lower effectiveness in those hybrid layers. A

separate conditioning step to improve the infiltration of self-etch adhesives through partially demineralized interfibrillar spaces has been recommended (Erhardt et al., 2011; Osorio et al., 2010), as phosphoric acid application augments dentin wettability due to an increase in dentin surface roughness and the opening and widening of dentin tubules. Therefore, a double conditioning effect is obtained.

In the clinical situation, resin-dentin interfaces are subjected to mechanical stress during chewing and swallowing (Frankenberger et al., 2005). *In vitro* load cycling has been shown to strongly inhibit matrix-metalloproteinases (MMPs) mediated collagen degradation in partially demineralized dentin, resulting in a decreased proteolysis of collagen due to tensile overloaded-induced action (Toledano et al., 2013). The interpretation of this fact is that mechanical loading enhances collagen´s resistance to enzymatic degradation in demineralized dentin. It could be speculated that a relationship between those findings and some process of a partial dentin remineralization, where mineral crystallites remaining within the collagen after partial demineralization might act as seed sites for apatite growth (Bertassoni et al., 2010). These hypotheses have been recently tested with some etch-and-rinse and two-step self-etching adhesives, using different research techniques as RAMAN, scanning electron microscopy or nanohardness measurements at the bonded interface (Toledano et al., 2014*a*; 2014*b*; 2014*c*, 2014*d*; 2014*e*).

Fluorescence microscopy has also been used to assess the interfacial morphology of the resin-dentin inter-diffusion zone and the distribution of dentin bonding agents, incorporating fluorescent markers prior to their application, highlighting the morphology and thickness of the hybrid layer formed in thin optical sections, with minimal preparation of the sample. This technique also allows visualization of resin tag extension, measurement

of adhesive layer thickness, and determination of possible defects or alterations at the bonded restoration interface (D'Alpino et al., 2006; de Oliveira et al., 2010). Micropermeability studies have revealed important information regarding bonded layer interfacial porosity, especially in samples apparently free of interfacial gaps. The extent of hybrid layer permeability is dependent on the penetration of adhesive components into etched dentin and on the development of porosities or gaps resulting from polymerization shrinkage of adhesives and/or resin components. Confocal laser scanning microscopy (CLSM) is capable of individually exciting different fluorochromes by applying selective wavelengths (Griffiths et al., 1999). CLSM allows to observe the ability of fluids to penetrate the interfacial region, thus verifying the presence of micropermeability in a bonded interface (D'Alpino et al., 2006; Sauro et al., 2012). Micropermeability correlates with the presence of porosities, and so with nanoleakage, whose clinical significance is unknown, but interfacial failures may occur if fluid is able to penetrate the interface and cause degradation of demineralized collagen fibres and adhesive monomers (Griffiths et al., 1999). Recently, a new method to assess dentin remineralization, based on the use of a calcium-chelator fluorophore, has been proposed (Profeta et al., 2013).

The aim of this study was to analyze the morphology and micropermeability of the dentin/adhesive interface using two different self-etching dentin adhesives with and without previous phosphoric acid etchant, after *in vitro* mechanical loading stimuli. The null hypothesis is that nanoleakage reduction and mineral precipitation are not produced at the resin-dentin interface after using previous acid etching and/or mechanical loading application.

MATERIAL AND METHODS.

a) *Samples preparation.*

Sixty four non-carious human third molars were obtained with informed consent from donors (20 to 40 yr of age; average: 31,9/SD: 5,4), under a protocol approved by the Institution review board. Molars were stored at 4 ºC in 0.5% chloramine T for up to 1 month before use. A flat mid-coronal dentin surface was exposed using a hard tissue microtome (Accutom-50; Struers, Copenhagem, Denmark) equipped with a slow-speed, water-cooled diamond wafering saw (330-CA RS-70300, Struers, Copenhagen, Denmark). A 180-grit silicon carbide (SiC) abrasive paper mounted on a water-cooled polishing machine (LaboPol-4, Struers, Copenhagem, Denmark) was employed to produce a clinically relevant smear layer (Koibuchi et al., 2001). Fifty per cent of the specimens were submitted to 37% phosphoric acid etching of dentin, for 10 seconds. Two adhesives from VOCO (VOCO GmbH, Cuxhaven Germany) were applied following manufacturer's instructions (Table 1): 1) Futurabond U and 2) experimental adhesive. A resin composite from VOCO, Grandio SO, was incrementally placed in five 1 mm layers and light-cured for 40s (Translux EC halogen light-curing unit (Kulzer GmbH, Bereich Dental, Wehrheim, Germany).

b) *Confocal microscopy evaluation.*

Previous to adhesive application, bond resins were doped with 0.05 wt% Rhodamine-B (Rh-B: Sigma-Aldrich ChemieGmbh, Riedstr, Germany). In 32 specimens, the pulpal chamber was filled with 1 wt% aqueous/ethanol fluorescein (Sigma-Aldrich ChemieGmbh, Riedstr, Germany) for 3 h (Toledano et al., 2013*b*; Sauro et al., 2012). The rest of the molars were immersed in 0.5 wt% xylenol orange solution (XO: Sigma-Aldrich

ChemieGmbh, Riedstr, Germany), excited at 514-nm for 24 h at 37 ºC (pH 7.2). The latter is a calcium-chelator fluorophore commonly used in hard tissues remineralization studies, due to its ability to form complexes with divalent calcium ions (Profeta el al., 2013). Specimens were copiously rinsed with water and treated in an ultrasonic water bath for 2 min. The specimens were cut in resin-dentin slabs and polished using ascending grit SiC abrasive papers (#1200 to #4000) on a water-cooled polishing device (Buehler-MetaDi, Buehler Ltd. Lake Bluff, IL, USA). A final ultrasonic cleaning (5 min) concluded the specimen preparation. Analysis of bonded interfaces were performed by dye assisted confocal microscopy evaluation (CLSM), and attained by using a confocal laser scanning microscope (SP5 Leica, Heidelberg, Germany) equipped with a 20x, 40x and 60x oil immersion lenses. Fluorescein is activated by blue light (488-495 nm) and emits yellow/green (520 nm), while the ultramorphology evaluation (resin-diffusion) was executed using Rhodamine excitation laser. Rhodamine is excited using green light (540 nm) and emits red in color (590 nm). CLSM images were obtained with a 1 μm z-step to optically section the specimens to a depth up to 12-10 μm below the surface. The z-axis scans of the interface surface was arbitrarily pseudo-colored by the same operator for better exposure and compiled into single projections using the Leica image-processing software SP2 (Leica, Heidelberg, Germany). The resolution of CLSM images was 1024 x 1024 pixels. Five optical images were randomly captured from each resin-dentin interface, and micrographs representing the most common features of nanoleakage observed along the bonded interfaces were selected (Toledano et al., 2013*a*; Profeta et al., 2013). Three specimens from each subgroup were immersed. Fluorescences were or not separated into spectral regions, allowing that the operator has a full control of the region of the light spectrum directed to each channel.

c) *Mechanical loading test.*

Half of the specimens of each experimental group were submitted to mechanical loading. To proceed with the mechanical cycling test, teeth were mounted in the load cycling machine [100,000 cycles, 3 Hz, 49 N (59-10 N)] (S-MMT-250NB; Shimadzu, Tokyo, Japan). The cycling compressive was applied to the flat resin composite build-ups using a 5-mm diameter spherical stainless steel plunger, while immersed in simulated body fluid (SBF) (Table 1). Specimens were then immersed in SBF, in order to complete a 24 h storage period. Non-loaded specimens were stored in SBF for 24 h. The other half of samples were stored in SBF, for 24 h. Table 2 reflects the groups of study.

RESULTS AND DISCUSSION.

Based on the results obtained in this study, the null hypothesis that nanoleakage reduction and mineral precipitation are not produced at the resin-dentin interface after using previous acid etching and/or mechanical loading application, must be rejected as load cycling implemented on the resin-dentin interfaces produced with two self-etching adhesives applied on previous PA-etched dentin surfaces promoted advance of sealing and mineralization of the resin-dentin interfaces.

In general, the CLSM analysis revealed that resin-dentin interfaces of unloaded specimens were deficiently resin-hybridized. At bonded interfaces created with Futurabond U adhesive applied on both smear layer-covered dentin (Fig 1) or PA-treated dentin surfaces (Fig 2), after multi-fluorescence examination, a rodhamine B-labeled hybrid complex and adhesive layer completely affected by fluorescein penetration (nanoleakage) through the porous resin-dentin interface (Figs 1B1, 2B1) was observed. Both were labeled at the same time, and resulted from combining specific filters after matching the excitation

line and the emission band. This technique permits assessing specimens that contain two fluorophores labeling different targets, observing each target separately, or at the same time. The advantage of simultaneous excitation is that the corresponding pixels of the two images are definitely in register because a single spot of incident light is the source of both of them (Pawley, 2006), allowing the overlapping between both original channels.

When adhesives were applied following the manufacturer instructions (without previous acid-etching), the adhesive was able to diffuse within the dentin creating a thin hybrid complex (Fig 1B1); after PA acid-etching, this hybrid zone was considerably thicker (Fig 2C1).The resin-dentin interface, when using self-etching mode, was characterized by scarce and short (Fig 1B2) or profuse medium-size resin tags (Fig 2C2), and micropermeability was detected several microns away from the adhesive layer (Figs 1B1, 2C1). The dentin interface presented funneled dentinal tubules (Fig 2C1); it is considered an essential sign of degradation of the poorly resin-infiltrated demineralized and peritubular dentin (Profeta et al., 2013), as it is observed after the evaluation of the fluorophore which labeled the Rhodamine as a separate target, matching the excitation line and the emission band (Pawley, 2006).This advance degree of degradation may be attributed to the high hydrophilicity of this interface, which may have permitted excessive water adsorption and induced severe resin degradation as well as the extraction of water-soluble unreacted monomers or oligomers from the resin matrix (Tay & Pashley, 2003). On the other hand, mild (Figs 5A1, 5B1) fluoroscein dye penetration (*i.e*., micropermeability) and water sorption (Fig 5B3) were observed within the resin infiltrated hybrid complex when the experimental adhesive was used; both figures exhibited an intense spectral overlap (yellow), in the emission of profile of both dyes (red and green), but funneling of the tubular orifices was not evident. Dentinal tubules adopted cylindrical shapes, with a good

penetration of the adhesive into the tubules and their lateral branches. This adhesive layer was also characterized by the presence of multiple short resin tags (Fig 5B2) (asterisk) and the diffusion of Rhodamine B along the tubules through the hybrid zone, and along the interface. Nevertheless, when the experimental adhesive was applied with previous phosphoric acid-etching, mild (Fig 6A1) or moderate (Fig 6C1) fluoroscein dye penetration (*i.e.*, micropermeability) and water sorption (Fig 6B3) were observed within the resin infiltrated hybrid complex (Fig 6C1). At Fig 6C1, a discrete spectral overlap (yellow) may be appreciated in the emission of profile of both dyes (red and green). Light funneling of the tubular orifices was evident with a good penetration of the adhesive into the tubules and their lateral branches. This adhesive layer was also characterized by the presence of long resin tags. Rhodamine B, similarly, passed along the tubules through the hybrid zone along the interface. Discontinuities in the tubular filling with primer or adhesive was also seen in this single labeled sample, indicating the intermittent passage of fluorescein from the lateral tubuli toward the main dentinal tubules.

In contrast, mechanical loading induced critical changes when both adhesives were utilized. Load cycling promoted an improved sealing of the resin-dentin interface at both intertubular and peritubular dentin, an increment of dentin mineralization, and a decrease of the hybrid complex porosity. It has been stated (Van Meerbeek et al., 2000) that porosity within the hybrid layer is the result of unpolymerized monomers that leach out and hydrolysis or degradation of collagen, among others. The resin-bonded dentin interface created with Futurabond U adhesive applied on smear layer-covered dentin and load cycled (Fig 3) showed less micropermeability and nanoleakage than the unloaded samples (Fig 1B). The fluorescein penetration achieved the adhesive layer through some more permeable dentinal tubules (Fig 3B1). The resin-dentin interface was characterized by scarce but long

resin tags (Fig 3B2). Fluorescein infiltrated the top of the rodhamine B-labeled hybrid complex throughout the tubules and the partially porous hybrid complex; discontinuities in the tubular filling with primer or adhesive could also be seen in this single labeled sample. Additionally, the resin-bonded dentin interface created with Futurabond U adhesive applied on PA-conditioned dentin and load cycled (Fig 4) showed less micropermeability (scarce porosities and nanoleakage) than the unloaded samples (Figs 2B1, 2C1). Fluorescein infiltrated the top of the rodhamine B-labeled hybrid complex throughout both the wall of the tubules and the partially porous hybrid layer. The fluorescein penetration stopped several microns away from a resin-dentin interface, characterized by short resin tags. The reason why only short resin tags could be created during this procedure is shown in Figs 4C1 and 4C4, where it is possible to observe a strong reflective signal from the beginning of the canaliculi, probably indicating the presence of mineral segments. This hypothesis was also validated when immersing the specimens in the xylenol orange solution (Profeta et al., 2013). In general, load cycled specimens treated with XO-dye produced a clearly outlined fluorescence due to a consistent Ca-minerals deposited within the bonding interface and inside the dentinal tubules. Futurabond U adhesive applied on smear layer-covered dentin after load cycling displayed some scarce and long resin tags (Fig 10B) below a very thin hybrid complex, though dentinal tubules appeared clearly stained with XO-dye, which showed a remarkable fluorescence signal (Fig 10C) due to consistent presence of Ca-minerals within the tubules and walls of dentinal tubules. This strong xylenol orange signal from the hybrid layer and the dentinal tubules clearly indicated the remineralization of these areas which were previously detected as mineral-deficient/poor-resin infiltrated zones of the resin-dentin interface. Moreover, the previous application of phosphoric acid, in this group (Fig 12), promoted a strong

fluorescence signal of XO-dye within the hybrid complex and wider dentinal tubules, revealing the presence of more abundant calcium complexes within both the partially demineralized dentin and dentinal tubules, which remineralized after mechanical loading (Smith, 2012). The clinical significance of these findings correlates with the formation of mineral precipitants within the interface (Fig 12A) which seal both the porosity of the hybrid complex and the non hybridized resin tags (Fig 2C1), protecting the exposed collagen fibers, reinforcing the resin-dentin interface and preventing bacterial colonization and pathogen-associated molecular complexes over time (Sauro et al., 2013).

When the experimental adhesive was applied on dentin, and then load cycled (Fig 7), scarce (Fig 7A1) or null (Fig 7B1) fluoroscein dye penetration (*i.e.*, micropermeability) and moderate water sorption (Figs 7A3 and 7B3) were observed within the resin infiltrated hybrid complex. Visible micropermeabilty and water sorption were noticeable within the dentinal tubules (Figs 7A1, 7B3). A slight and thin signal of dye penetration was observed over the adhesive layer (7A1) and through the adhesive layer (7B1). In the CLSM image captured in fluorescence (fluorescein excitation/emission only) it was possible to observe an adhesive layer characterized by the presence of a few wide and long resin tags, when imaged in Rhodamine excitation/emission mode (Figs 7B1, 7B2). A faint reflective signal inside the dentinal tubules was also observed (7B4), indicating the presence of partially obliterating mineral segments, as confirmed the XO-dye microanalysis. When the experimental adhesive was examined after load cycling it was possible to observe an adhesive layer characterized by the presence of larger and less redder resin tags, when imaged in Rhodamine excitation/emission mode (Figs 14A, 14B). Moderate and discontinuous fluorescence signal of XO-dye within both the hybrid complex, and some dentinal tubules, could also be detected. The strongest presence of XO-dye bonded to both

the hybrid complex and the dentinal tubules content was observed when the experimental adhesive was applied on phosphoric acid-etched dentin and then load cycled (Figs 16A, 16C). Clear dentin remineralization, determined as a strong calcium-deposition, was observed within those locations, as detectable mineral precipitations both on the surface and inside the dentinal tubules were confirmed. We hypothesize that the therapeutic remineralizing effects observed within the mineral depleted resin-dentin interface were essentially due to bioactivity of these loading stimuli (Toledano et al., 2014*f*, 2014*g*).

Similarly, when phosphoric acid was firstly applied, scarce fluoroscein dye penetration (Fig 8B1) (*i.e.*, micropermeability) and water sorption (Fig 8B3) were observed within the resin infiltrated hybrid complex. Moderate micropermeabilty was also detected within the dentinal tubules (Figs 8B1, 8B3, 8C1, 8C3). A complete signal of dye penetration was shown over the adhesive layer (Fig 8C1) and through the adhesive layer (Fig 8C3). In the CLSM image captured in fluorescence (fluorescein excitation/emission only) it was possible to observe an adhesive layer characterized by the presence of mostly wide and short resin tags, when imaged in Rhodamine excitation/emission mode (Figs 8B2, 8C2). A strong reflective signal from the bottom of the hybrid complex and inside the dentinal tubules was detected (8A4, 8B4), suggesting the presence of some solid and obliterating mineral segments, and confirmed through the xylenol orange analysis; a clear fluorescence signal due to consistent presence of xilenol-stained Ca-deposits within the hybrid complex, walls of dentinal tubules and resin tags were exposed (Fig 16C).

Durability of the resin-dentin interface represents one of the main concerns in adhesive dentistry as it is affected by severe degradation. This occurs mainly via water sorption and hydrolysis of monomer methacrylates ester bonds caused by salivary esterases

(Moszner et al, 2005). Unloaded samples, occasionally, showed a brief and limited XO-dye at the top of the resin-dentin interface, and in the first microns of resin tags length, interpreted as a slight fluorescence signal, due to the higher hydrophilicity of the resin components which uptake water and Ca from the SBF solution. The uptake kinetics of cation exchange is fast in the presence of Na, as the predominant exchangeable cation can result in material swelling (Profeta et al., 2013). At the moment, some disadvantages of water-based, highly acidic self-etching dentin adhesives, in particular single-bottle adhesives arise from the hydrolytic instability of the methacrylate monomers used. Bisphenol A diglycidyl ether dimethacrylate (Bis-GMA) and urethane-dimethacrylates (UDMA) are most frequently used as hydrophobic cross-linkers in adhesive systems, providing mechanical strength to the adhesive, thus preventing substantial water uptake after curing of the adhesive resin. Nevertheless, some water sorption is inevitable due to the polar ether-linkages and/or hydroxyl groups (Sideridou et al., 2002). 2-hydroxyrthyl methaxrylate (HEMA), a small monomer widely used in dentistry, is very frequently added to adhesives not only to ensure good wetting, but also because of its solvent-like nature (Van Landuyt et al., 2007). One of the most important characteristics of HEMA is its hydrophilicity, making it an excellent adhesion-promoting monomer (Nakabayashi et al., 1992), but both in uncured and cured state, HEMA will readly absorb water, which can lead to dilution of the monomers to the extent that polymerization is inhibited (Jacobsen & Söderholm, 1995). Moreover, HEMA fixed in a polymer chain after polymerizing will still exhibit hydrophilic properties and will lead to water uptake, resulting in the formation of water trees at the interface (Tay et al., 2002) with consequent swelling and discoloration (Burrow et al., 1999). Thereby, hydroxyethyldimethacrylate (HEDMA), some other regular methacrylate and highly hydrophilic monomers present in Futurabond U, have not been

incorporated into the chemical formulation of the experimental adhesive for resin-dentin preservation purposes.

These findings were corroborated by a slight signal of XO stain that was observed not only over the hybrid complex and within some dentinal tubules when Futurabond U was applied on smear layer-covered dentin (9A, 9C), but when phosphoric acid was previously applied (Fig 11C). When imaged in Rhodamine excitation/emission mode, long resin tags were discernible underneath the adhesive layer and hybrid complex (9B). Specimens treated with acid before Futurabond U application exhibited XO-dye staining the first 10-20 μm of resin tags; the rest of resin-tags length showed the typical Rodhamine B-labeled colorant (Fig 11A). The resin-dentin interface promoted by the experimental adhesive applied on smear layer-covered dentin denoted the presence of an interface made of a compact hybrid complex, and multiple resin tags (Figs 13A, 13B) imaged in Rhodamine excitation/emission mode, and a faint XO-dye was observed in some canaliculi. On the contrary, good penetration of the experimental adhesive into the phosphoric acid-treated dentin surface and tubules was observed (Fig 15). Short and robust resin tags stained with xylenol orange evidenced the sealing of the resin-dentin interface. Some empty dentinal tubules appeared below the XO-dye resin tags, though with Rhodamine B infiltrating the intertubular dentin.

Two fundamental concepts to prevent the degradation of resin-dentin interfaces and increase their longevity are required, (1) replacement of the dentin-mineral phase to protect the collagen from biodegradation, and (2) reduction of the water-filled regions at the bonding interfaces (micro/nano porosities) (Sauro et al., 2013). As result of the present work, *in vitro* load cycling promoted advanced sealing and mineralization at the resin-infiltrated dentin and mineral depleted areas at the underlying dentin, after using both

single-bottle self-etching dentin adhesives, evoking reparative processes via apatite deposition within the mineral-depleted dental hard tissues (Kokubo & Takadama, 2006). A wide range of growth factors and matrix signaling molecules can be released or activated in dentin at sites of loading, remodeling and contributing to further tissue genesis and regeneration. These bioactive molecules become immobilized within the matrix, where they become fossilized in a protected stage thorough the interaction with other molecules and the mineral of the extracellular matrix (Smith et al., 2012). *In vivo* and *in vitro* intermittent compressive load stimulates the alkaline phosphatase activity (Mc Allister & Frangos, 1999; Li et al., 2011; Reijnders et al., 2013; Lozupone et al., 1996). Alkaline phosphatase, present at all mineralization sites, hydrolyses phosphate esters producing free phosphate (Posner et al., 1986), essential for normal development, maintenance and repair of teeth. Additionally, this increase of alkalinity and the new hydroxyapatite formation may also have interfered with the activity of MMPs (Osorio et al., 2014). On the other hand, reparative and reactionary dentin form in response to external stimuli, teeth injuries and dental caries. Stimuli as mechanical loading, injury and trauma can easily increase the pulpal hydrostatic pressure of the dentin structure. This pressure gradient (14-70 cm H_2O) from mechanical loading may increase interstitial fluid (Mc Allister & Frangos, 1999), fluid flow, which has been shown to have an important role in load-induced hard-tissue remodeling. This common occurrence can lead to some appropriate inductive molecular signals associated to an increase of calcified nodules and local amount of calcium, promotes calcium phosphate formation and stimulates matrix formation and mineralization (Li et al., 2011). Mechanical loading and fluid flow stimulate nitric oxide, which mediates signal transduction in hard tissues. Flow-induced nitric oxide is biphasic, with a G-protein- and calcium-dependent burst associated with the onset of flow, and a G-protein- and

calcium-independent phase associated with or steady sustained flow (Mc Allister & Frangos, 1999).

A combined Fluorescein/Rhodamine and XO CLSM analysis demonstrated that the experimental self-etching adhesive produced a more advanced degree of sealing and mineralization capability of the resin dentin interface. Both adhesives incorporate a water/ethanol mixture, as solvent (Table 1). But there is an important difference between them, Futurabond U requires mixing and stirring thoroughly of two liquids, that practically takes around 15 s. In water/ethanol mixtures, the evaporation rate of ethanol is extremely high (Spedding et al., 1993); it may be complete even after 6 to 10 s (Innocenzi et al., 2008). Therefore, it is possible than when Futurabond U is applied on wet dentin, ethanol concentration is highly reduced. On the contrary, the experimental adhesive requires no mixing, and solvent concentration will not be altered when applied to dentin. Water is a strongly polar solvent with a high dielectric constant, capable of dissolving ionic lattices and polar compounds, determined by its capability of forming strong hydrogen bonds. However, as water is a poor solvent for organic compounds, as monomers, a secondary solvent such as ethanol is required to improve adhesive efficiency (Van Landuyt et al., 2007). Water-alcohol mixtures are known to be azootropic (Moszner et al., 2005), which results in more water removal from the adhesive, increasing surface dehydration, avoiding water blisters (Tay et al., 1998) and improving the bonding efficacy (Pashley et al.,1998). Even more, ethanol maintains wide interfibrillar spaces after evaporation of the solvent, improving resin infiltration and quality of dentin bonding (Carvalho et al., 2003). Incorporation of water/ethanol as solvents into the chemical formulation of the experimental adhesive might have, as a consequence, improved bonding and advanced dentin mineralization.

SUMMARY

The resin-dentin interface, when using self-etching mode presented essential sign of degradation of the poorly resin-infiltrated demineralized and peritubular dentin, attributed to the thigh hydrophilicity of this interface, which permitted excessive water adsorption. In general, the CLSM analysis revealed that resin-dentin interfaces of unloaded specimens were deficiently resin-hybridized. Load cycling promoted an improved sealing of the resin-dentin interface at both intertubular and peritubular dentin, an increment of dentin mineralization, and a decrease of the hybrid complex porosity. Load cycling implemented on the resin-dentin interfaces produced with two self-etching adhesives applied on previous PA-etched dentin surfaces produced advance of sealing and mineralization of the resin-dentin interfaces. The resin-bonded dentin interface created with Futurabond U adhesive applied on PA-conditioned dentin and load cycled showed less micropermeability (scarce porosities and nanoleakage) than the unloaded samples; these specimens showed strong reflective signal from the beginning of the canaliculi, probably indicating the presence of mineral segments. This mineralization was confirmed after observing a strong fluorescence signal of XO-dye within the hybrid complex and wider dentinal tubules. This therapeutic effect correlates with the formation of mineral precipitants within the interface which seal both the porosity of the hybrid complex and the non hybridized resin tags protecting the exposed collagen fibers, reinforcing the resin-dentin interface and preventing bacterial colonization and pathogen-associated molecular complexes over time. When the experimental adhesive was applied after phosphoric acid and then load cycled, clear dentin remineralization was determined as a solid calcium-deposition and obliterating mineral segments, associated to the strongest presence of XO-dye bonded to both the hybrid complex and the dentinal tubules content. As result of the present work, *in vitro* load

cycling promoted advanced sealing and mineralization at the resin-infiltrated dentin and mineral depleted areas at the underlying dentin, after using both single-bottle self-etching dentin adhesives, evoking reparative processes via apatite deposition within the mineral-depleted dental hard tissues. The combined Fluorescein/Rhodamine and XO CLSM analysis demonstrated that the experimental self-etching adhesive produced a more advanced degree of sealing and mineralization capability of the resin dentin interface.

ACKNOWLEDGEMENTS

This work was supported by grants MINECO/FEDER MAT2011-24551, MAT2014-52036-P, and CEI-Biotic UGR. The authors have no financial affiliation or involvement with any commercial organization with direct financial interest in the materials discussed in this manuscript. Any other potential conflict of interest is disclosed.

REFERENCES

BERTASSONI, L.E., HABELITZ, S., PUGACH, M., SOARES, P.C., MARSHALL, S.J. & MARSHALL JR., G.W. (2010). Evaluation of surface structural and mechanical changes following remineralisation of dentin. *Scanning* **32**, 312–319.

BURROW, M.F., INOKOSHI, S. & TAGAMI, J. (1999). Water sorption of several bonding resins. *Am J Dent* **12**, 295-298.

CARVALHO, R.M., MENDONÇA, J.S., SANTIAGO, S.L., SILVEIRA, R.R., GARCIA, F.C., TAY, F.R. & PASHLEY, D.H. (2003). Effects of HEMA/solvent combinations on bond strength to dentin. *J Dent Res* **82,** 597-601.

D'ALPINO, P.H., PEREIRA, J.C., SVIZERO, N.R., RUEGGEBERG, F.A. & PASHLEY, D.H. (2006). Factors affecting use of fluorescent agents inidentification of resin-based polymers. *J Adhes Dent* **8**, 285-292.

DE MUNCK, J., MINE, A., VAN DEN STEEN, P.E., VAN LANDUYT, K.L., POITEVIN, A., OPDENAKKER, G. & VAN MEERBEEK, B. (2010). Enzymatic degradation of adhesive-dentin interfaces produced by mild self-etch adhesives. *Eur J Oral Sci* **118**, 494-501.

DE OLIVEIRA, M.T., ARRAIS, C.A., ARANHA, A.C., DE PAULA EDUARDO, C., MIYAKE, K., RUEGGEBERG, F.A. & GIANNINI, M. (2010). Micromorphology of resin-dentin interfaces using one-bottle etch&rinse and self-etching adhesive systems on laser-treated dentin surfaces: a confocal laser scanning microscope analysis. *Lasers Surg Med* **42**, 662-670.

ERHARDT, M.C., PISANI-PROENÇA, J., OSORIO, E., AGUILERA, F.S., TOLEDANO, M. & OSORIO, R. (2011). Influence of laboratory degradation methods and bonding

application parameters on microTBS of self-etch adhesives to dentin. *Am J Dent* **24**, 103-108.

FRANKENBERGER, R., PASHLEY, D.H., REICH, S.M., LOHBAUER, U., PETSCHELT, A. & TAY, F.R. (2005). Characterisation of resin–dentineinterfaces by compressive cyclic loading. *Biomaterials* 26, 2043–2052.

GRIFFITHS, B.M., WATSON, T.F. & SHERRIFF, M. (1999). The influence of dentinebonding systems and their handling characteristics on themorphology and micropermeability of the adhesive interface. *J Dent* **27**, 63–71.

INNOCENZI, P., MALFATTI, L., COSTACURTA, S., KIDCHOB, T., PICCININI, M. & MARCELLI, A. (2008). Evaporation of ethanol and ethanol-water mixtures studied by time-resolved infrared spectroscopy. *J Phys Chem A **112***, 6512-6516.

JACOBSEN, T. & SÖDERHOLM, K.J. (1995). Some effects of water on dentin bonding. *Dent Mater* **11**, 132-136.

KOIBUCHI, H., YASUDA, N. & NAKABAYASHI, N. (2001). Bonding to dentin with a self-etching primer: the effect of smear layers. *Dent Mater* **17**, 122–126.

KOKUBO, T. & TAKADAMA, H. (2006). How useful is SBF in predicting in vivo bone bioactivity? *Biomater* **27,** 2907-2915.

LI, L., ZHU, Y.Q., JIANG, L., PENG, W. & RITCHIE, H.H. (2011). Hypoxia promotes mineralization of human dental pulp cells. *J Endod* **37**, 799-802.

LOZUPONE, E., PALUMBO, C., FAVIA, A., FERRETTI, M., PALAZZINI, S. & CANTATORE, F.P. (1996). Intermittent compressive load stimulates osteogenesis and improves osteocyte viability in bones cultured "in vitro". *Clin Rheumatol* **15**, 563-572.

MCALLISTER, T.N. & FRANGOS, J.A. (1999). Steady and transient fluid shear stress stimulate NO release in osteoblasts through distinct biochemical pathways. *J Bone Miner Res* **14**, 930-936.

MOSZNER, N., SALZ, U. & ZIMMERMANN, J. (2005). Chemical aspects of self-etching enamel-dentin adhesives: a systematic review. *Dent Mater* **21**, 895-910.

NAKABAYASHI, N. & SAIMI, Y. (1996). Bonding to intact dentin. *J Dent Res* **75**, 1706-1715.

NAKABAYASHI, N., WATANABE, A. & GENDUSA, N.J. (1992). Dentin adhesion of "modified"4-META/MMA-TBB resin: function of HEMA. *Dent Mater* **8**, 259-264.

OSORIO, R., OSORIO, E., AGUILERA, F.S., TAY, F.R., PINTO, A. & TOLEDANO, M. (2010). Influence of application parameters on bond strength of an "all in one" water-based self-etching primer/adhesive after 6 and 12 months of water aging. *Odontology* **98**, 117-125.

OGURI, M., YOSHIDA, Y., YOSHIHARA, K., MIYAUCHI, T., NAKAMURA, Y., SHIMODA, S., HANABUSA, M., MOMOI, Y. & VAN MEERBEEK, B. (2012). Effects of functional monomers and photo-initiators on the degree of conversion of a dental adhesive. *Acta Biomater* **8**, 1928-1934.

OSORIO, R., OSORIO, E., CABELLO, I., TOLEDANO, M. (2014). Zinc induces apatite and scholzite formation during dentin remineralization. *Caries Res* **48,** 276-290.

PASHLEY, E.L., ZHANG, Y., LOCKWOOD, P.E., RUEGGEBERG, F.A. & PASHLEY, D.H. (1998). Effects of HEMA on water evaporation from water-HEMA mixtures. *Dent Mater* **14**, 6-10.

PAWLEY, J.B. (2006). *Handbook of biological confocal microscopy*. Maddison, USA: Springer.

POSNER, A.S., BLUMENTHAL, N.C. & BOSKEY, A.L. (1986). Model of aluminum-induced osteomalacia: inhibition of apatite formation and growth. *Kidney Int* **18**, S17-S19.

PROFETA, A.C., MANNOCCI, F., FOXTON, R., WATSON, T.F., FEITOSA, V.P., DE CARLO, B., MONGIORGI, R., VALDRÉ, G. & SAURO, S. (2013). Experimental etch-and-rinse adhesives doped with bioactive calcium silicate-based micro-fillers to generate therapeutic resin-dentin interfaces. *Dent Mater* **29**, 729-741.

REIJNDERS, C.M., VAN ESSEN, H.W., VAN RENS, B.T., VAN BEEK, J.H., YLSTRA, B., BLANKENSTEIN, M.A., LIPS, P. & BRAVENBOER, N. (2013). Increased Expression of Matrix Extracellular Phosphoglycoprotein (MEPE) in Cortical Bone of the Rat Tibia after Mechanical Loading: Identification by Oligonucleotide Microarray. *PLoS One* **8**, e79672.

SAURO, S., OSORIO, R., WATSON, T.F. & TOLEDANO, M. (2012). Therapeutic effects of novel resin bonding systems containing bioactive glasses on mineral-depleted areas within the bonded-dentin interface. *J Mater Sci Mater Med* **23**, 1521–1532.

SAURO, S., OSORIO, R., FULGENCIO, R., WATSON, T.F., CAMA, G., THOMPSON, I. & TOLEDANO, M. (2013). Remineralisation properties of innovative light-curable resin-based dental materials containing bioactive micro-fillers. *J Mater Chem B* **1**, 2624-2638.

SIDERIDOU, I., TSERKI, V. & PAPANASTASIOU, G. (2002). Effect of chemical structure on degree of conversion in light-cured dimethacrylate-based dental resins. Biomaterials **23**, 1819-1829.

SMITH, A.J., SCHEVEN, B.A., TAKAHASHI, Y., FERRACANE, J.L., SHELTON, R.M. & COOPER, P.R. (2012). Dentin as a bioactive extracellular matrix. *Arch Oral Biol* **57**, 109-121.

SPEDDING, P.L.,GRIMSHAW, J. & O´HARE, K.D. (1993). Abnormal evaporation rate of ethanol from low concentration aqueous solutions. *Langmuir* **9,** 1408-1413.

SPENCER, P., YE, Q., PARK, J., TOPP, E.M., MISRA, A., MARANGOS, O., WANG, Y., BOHATY, B.S., SINGH, V., SENE, F., ESLICK, J., CAMARDA, K. & KATZ, J.L. (2010). Adhesive/dentin interface: the weak link in the composite restoration. *Ann Biomed Eng* **38**, 1989-2003.

TAY, F.R., GWINNETT, J.A. & WEI, S.H. (1998). Relation between water content in acetone/alcohol-based primer and interfacial ultrastructure. *J Dent* **26**, 147-156.

TAY, F.R., GWINNETT, J.A. & WEI, S.H. (1996). Micromorphological spectrum from overdrying to overwetting acid-conditioned dentin in water-free acetone-based, single-bottle primer/ adhesives. *Dent Mater* **12**, 236-244.

TAY, F.R., PASHLEY, D.H., SUH, B.I., CARVALHO, R.M. & ITTHAGARUN, A. (2002). Single-step adhesives are permeable membranes. *J Dent* **30**, 371-382.

TAY, F.R. & PASHLEY, D.H. (2003). Have dentin adhesives become too hydrophilic? *J Can Dent Assoc* **69**, 726-731.

TOLEDANO, M., YAMAUTI, M., RUIZ-REQUENA, M.E & OSORIO R. (2012). ZnO-doped adhesive reduced collagen degradation favouring dentin remineralisation. *J Dent* **40**, 756-765.

TOLEDANO, M., AGUILERA, F.S., YAMAUTI, M., RUIZ-REQUENA, M.E. & OSORIO, R. (2013). In vitro load-induced dentin collagen-stabilization against MMPs degradation. *J Mech Behav Biomed* **27**, 10-18.

TOLEDANO, M., OSORIO, E., AGUILERA, F.S., SAURO, S., CABELLO, I. & OSORIO, R. (2014*a*). In vitro mechanical stimulation promoted remineralization at the resin/dentin interface. *J Mech Behav Biomed Mater* **30**, 61-74.

TOLEDANO, M., AGUILERA, F.S., SAURO, S., CABELLO, I., OSORIO, E. & OSORIO, R. (2014*b*). Load cycling enhances bioactivity at the resin-dentin interface. *Dent Mater* **30**, e169-e188.

TOLEDANO, M., AGUILERA, F.S., CABELLO, I. & OSORIO, R. (2014*c*). Remineralization of mechanical loaded resin-dentin interface: a transitional and synchronized multistep process. *Biomech Model Mechanobiol* **13**,1289-1302.

TOLEDANO, M., AGUILERA, F.S., OSORIO, E., CABELLO, I. & OSORIO, R. (2014*d*). Microanalysis of Thermal-Induced Changes at the Resin-Dentin Interface. *Microsc Microanal* **6**, 1-16.

TOLEDANO, M., AGUILERA, F.S., CABELLO, I. & OSORIO, R. (2014*e*). Masticatory function induced changes, at subnanostructural level, in proteins and mineral at the resin-dentine interface. *J Mech Behav Biomed Mater* **39**, 197-209.

TOLEDANO, M., CABELLO, I., AGUILERA, F.S., OSORIO, E., & OSORIO, R. (2014*f*). Effect of *in vitro* chewing and bruxism events on remineralization, at the resin-dentin interface. *J Biomech*. doi: 10.1016/j.jbiomech.2014.11.014.

TOLEDANO, M., AGUILERA, F.S., OSORIO, E., CABELLO, I., TOLEDANO-OSORIO, M. & OSORIO, R. (2014*g*). Bond strength and bioactivity of Zn-doped dental adhesives promoted by load cycling. *Microsc Microanal* **11**, 1-17.

VAN LANDUYT, K.L., SNAUWAERT, J., DE MUNCK, J., PEUMANS, M., YOSHIDA, Y., POITEVIN, A., COUTINHO, E., SUZUKI, K., LAMBRECHTS, P. & VAN MEERBEEK, B. (2007). Systematic review of the chemical composition of contemporary dental adhesives. *Biomaterials* **28**, 3757-3785.

VAN MEERBEEK, B., VARGAS, M., INOUE, S., YOSHIDA, Y., PERDIGÃO, J., LAMBRECHTS, P. & VANHERLE, G. (2000). Microscopy investigations. Techniques, results, limitations. *Am J Dent* **13**, 3D-18D.

Table 1. Materials and chemicals used in this study and respective manufacturers, basic formulation and mode of application.

Product details	**Basic formulation**	**Mode of application**
Futurabond U (VOCO, Cuxhaven, Germany) (pH=2.3)	Liquid 1: Acidic adhesive monomer HEMA Bis-GMA HEDMA UDMA Catalyst Liquid 2: Ethanol Initiator Catalyst	**Dentin conditioning** 37% H_3PO_4 (15 s) Rinse with water Air-dry (5s) **Adhesive application** 1. Mix and stir thoroughly both liquids with the Single Tim applicator. 2. Apply the adhesive homogenously to the surface and rub for 20 s using the Single Tim. 3. Dry off the adhesive layer with dry, oil-free air for at least 5 s. 4. Light cure the adhesive layer for 10 s.
Experimental adhesive (VOCO, Cuxhaven, Germany) (pH=2.3)	HEMA Bis-GMA Acidic adhesive monomers UDMA Ethanol/water	**Dentin conditioning** 37% H_3PO_4 (15 s) Rinse with water Air-dry (5s) **Adhesive application** 1. Apply the adhesive homogenously to the surface and rub for 20 s using the Single Tim. 2. Dry off the adhesive layer with dry, oil-free air for at least 5 s. 3. Light cure the adhesive layer for 10 s.
Phosphoric acid 37% (Braun Medical SA, Barcelona, Spain).		
Grandio SO (VOCO, Cuxhaven, Germany)	*Filler configuration* 0.5-3 µm particles; 20-40 nm nanoparticles *Matrix composition* Bis-GMA Bis-EMA TEGDMA	
SBFS (pH=7.45)	NaCl 8.035 g $NaHCO_3$ 0.355 g KCl 0.225 g	

	$K_2HPO_4 \cdot 3H_2O$ 0.231 g, $MgCl_2 \cdot 6H_2O$ 0.311 g 1.0 M – HCl 39 ml $CaCl_2$ 0.292 g Na_2SO_4 0.072 g Tris 6.118 g 1.0 M – HCl 0–5 ml	

Abbreviations: HEMA: 2-hydroxyethyl methacrylate; Bis-GMA: bisphenol A diglycidyl methacrylate; HEDMA: hydroxyethyldimethacrylate; UDMA: urethane dimethacrylate: H_3PO_4: phosphoric acid; Bis-EMA: ethoxylated bisphenol A glycol dimethacrylate; TEGDMA: triethylene glycol dimethacrylate; SBFS: simulated body fluid solution; NaCl: sodium chloride; $NaHCO_3$: sodium bicarbonate; KCl: potassium chloride; $K_2HPO_4 \cdot 3H_2O$: potassium phosphate dibasic trihydrate; $MgCl_2 \cdot 6H_2O$: magnesium chloride hexahydrate; HCl: hydrogen chloride; $CaCl_2$: Calcium chloride; Na_2SO_4: sodium sulfate; Tris: tris(hydroxylmethyl) aminomethane.

Table 2

Table of cases

Figure number	Adhesive	Challenge	Dye
1	Futurabond U	no PA-etch, no load-cycling	Rd/Fl
2	Futurabond U	PA-etch, no load-cycling	Rd/Fl
3	Futurabond U	no PA-etch, load-cycling	Rd/Fl
4	Futurabond U	PA-etch, load-cycling	Rd/Fl
5	Experimental	no PA-etch, no load-cycling	Rd/Fl
6	Experimental	PA-etch, no load-cycling	Rd/Fl
7	Experimental	no PA-etch, load-cycling	Rd/Fl
8	Experimental	PA-etch, load-cycling	Rd/Fl
9	Futurabond U	no PA-etch, no load-cycling	Rd/Xo
10	Futurabond U	no PA-etch, load-cycling	Rd/Xo
11	Futurabond U	PA-etch, no load-cycling	Rd/Xo
12	Futurabond U	PA-etch, load-cycling	Rd/Xo
13	Experimental	no PA-etch, no load-cycling	Rd/Xo
14	Experimental	no PA-etch, load-cycling	Rd/Xo
15	Experimental	PA-etch, no load-cycling	Rd/Xo
16	Experimental	PA-etch, load-cycling	Rd/Xo

Abreviations: PA: Phosphoric Acid; Rd: Rhodamine B; Fl: fluorescein; Xo: Xylenol orange

FIGURE LEGENDS

Figure 1. CLSM images (reflexion/fluorescence) showing the interfacial characterization and micropermeability of the resin-dentin interface created using Futurabond U adhesive applied on smear layer-covered dentin, and obtained at 40x (A) and 63x (B), with 100 and 25 μm of scale bars, respectively. Figs 1A1 and 1B1 show a generalized pattern of severe micropermeability and water sorption (arrows) at both adhesive layer (a) and dentinal tubules (t) (Figs 1B1, 1B3). A porous hybrid complex and a moderate nanoleakage signal from the hybrid complex (pointer) located underneath the Rhodamine B-labeled adhesive layer may be observed (Fig 1B1). In the CLSM image captured in fluorescence mode, it is possible to observe an adhesive layer characterized by the presence of many incipient, wide and short resin tags (rt) when imaged in Rhodamine excitation/emission mode (1B2) underneath the adhesive layer and a profuse dye sorption throughout its thickness when imaged in fluorescein excitation/emission mode (Fig 1B3). It is possible to observe a clear hybrid complex (hc) of approximate 0.2-1 μm thick. Funnelling (f) of the tubular orifices is observable, with good penetration of the adhesive (a) into the entrance of tubules (t). a, adhesive layer; d, dentin; f, funneling; hc, hybrid complex; rt, resin tags; t, dentinal tubules.

Figure 2. CLSM images (reflexion/fluorescence) showing the interfacial characterization and micropermeability of the resin-dentin interface created using Futurabond U adhesive applied on phosphoric acid-etched dentin, and obtained at 40x (A), 63x (B), and 63x-2 optical zoom (C), with 100, 25 and 10 μm of scale bars, respectively. Figs 2A1 and 2B1 show a generalized pattern of severe micropermeability (arrows) between dentin (d) and the adhesive layer (a). A porous HL and an intense nanoleakage signal from the hybrid layer (pointer) located underneath the Rhodamine B-labeled adhesive layer may be observed (Fig 2C1). In the CLSM image captured in fluorescence mode, it is possible to observe an adhesive layer characterized by the presence of many middle-size and short resin tags (rt) when imaged in Rhodamine excitation/emission mode (Fig 2C2) underneath the adhesive layer and a profuse dye sorption throughout its thickness when imaged in fluorescein excitation/emission mode (Fig 2C3). It is possible to observe a clear hybrid complex (hc) of approximate 4 μm thick. Funnelling (f) of the tubular orifices is evident with good penetration of the adhesive (a) into the tubules and their lateral branches (lb). a, adhesive layer; d, dentin; f, funneling; hc, hybrid complex; lb, lateral branches; rt, resin tags; t, dentinal tubules.

Figure 3. CLSM images (reflexion/fluorescence) showing the interfacial characterization and micropermeability of the resin-dentin interface created using Futurabond U adhesive applied on smear layer-covered dentin and then load cycled, and obtained at 40x (A) and 63x (B), with 100 and 25 μm of scale bars, respectively. At Figs 3A1 and 3B1 may be detected micropermeability localized at some dentinal tubules (arrow) (Figs 3A1, 3B1 and 3B3). The resin-dentin interface appears partially sealed by the adhesive (a), but with a regular dye sorption throughout its thickness. A brief reflective signal may be described at

dentin (d) (Fig 3B4) (asterisc). The adhesive layer is characterized by the presence of few long but scarce resin tags (rt) when imaged in fluorescence mode (Rhodamine excitation/emission) (Fig 3B2) and by a visible dye sorption throughout the *canaliculi* lumens (Fig 2B3) (arrow). In fluorescence mode (fluorescein excitation /emission), water sorption within the thickness of the adhesive can be seen (3A1, 3B1). It is possible to observe a well marked hybrid complex (approximate thickness 1 μm). Slight funnelling (f) of the tubular orifices is evident with good penetration of the adhesive (a) into the tubules. a, adhesive layer; d, dentin; f, funneling; hc, hybrid complex; rt, resin tags; t, dentinal tubules.

Figure 4. CLSM images (reflexion/fluorescence) showing the interfacial characterization and micropermeability of the resin-dentin interface created using Futurabond U adhesive applied on phosphoric acid-etched dentin and then load cycled, and obtained at 40x (A), 63x (B), and 63x-2 optical zoom (C), with 100, 25 and 10 μm of scale bars, respectively. Figs 4A1 and 4B1 show micropermeability (arrow) specially localized between some resin tags and tubule walls. At Fig 4C, it is shown a sealed interface by the adhesive (a), but with a tight dye sorption throughout its thickness (pointer). A strong reflective signal may be described from the bottom of the hybrid complex and inside the dentinal tubules (4B4, 4C4) (asterisc). The adhesive layer is characterized by the presence of thin and short (4A2, 4B2) or scarce and reduced (4C2) resin tags (rt) when imaged in fluorescence mode (Rhodamine excitation/emission) and by a tight (4A3, 4B3) or reduced (4C3) dye sorption throughout the *canaliculi* lumens. In fluorescence mode (fluoroscein excitation /emission), water sorption within the thickness of the adhesive can be seen (4B3, 4C3). It is possible to observe a well marked hybrid complex (approximate thickness of 4 μm). Funnelling (f) of

the tubular orifices is evident with good penetration of the adhesive (a) into the tubules and their lateral branches (lb) (Fig 4C1). a, adhesive layer; d, dentin; f, funneling; hc, hybrid complex; rt, resin tags; t, dentinal tubules.

Figure 5. CLSM images (reflexion/fluorescence) of the resin-dentin interface created using the experimental adhesive applied on smear layer-covered dentin, and obtained at 40x (A) and 63x (B) with 100 and 50 μm of scale bars respectively. It is shown an extended micropermeability (arrow) throughout all hybrid complex. A clear nanoleakage signal from the hybrid complex located underneath the adhesive layer may also be observed. In the CLSM image captured in fluorescence, it is possible to detect an adhesive layer characterized by the presence of multiple and cylindrical resin tags (rt) when imaged in Rhodamine excitation/emission mode (5B2) (asterisk), and by a clear dye sorption throughout their thickness (5B3). This resin infiltration is also characterized by a discrete reflective signal at both hybrid complex and inside the dentinal tubules (5B4) (arrow). a, adhesive layer; d, dentin; f, funneling; hc, hybrid complex; rt, resin tags; t, dentinal tubules.

Figure 6. CLSM images (reflexion/fluorescence) of the resin-dentin interface created using the experimental adhesive applied on PA-conditioned dentin, and obtained at 40x (A), 63x (B), and 63x-2 optical zoom (C), with 100, 25 and 10 μm of scale bars, respectively. A little and diffuse micropermeability (arrow) between the adhesive layer (a) and the resin composite (rc) may be shown. Some nanoleakage signal from the hybrid layer located underneath the adhesive layer may be observed. In the CLSM image captured in fluorescence, it is possible to notice an adhesive layer characterized by the presence of long resin tags (rt) when imaged in Rhodamine excitation/emission mode and by a faint dye

sorption throughout their thickness (Figs 6B1, 6C1). This resin infiltration is also characterized by an indiscernible reflective signal at both hybrid layer and inside the dentinal tubules (Figs 6B4, 6C4), though at low magnification (Fig 6A4) some mineral segments may be observed (Fig 6A1). a, adhesive; hc, hybrid complex; rc, resin composite; rt, resin tags.

Figure 7. The interfacial characterization and micropermeability of the resin-dentin interface created using the experimental adhesive applied on smear layer-covered dentin and then load cycled is shown at CLSM images (reflexion/fluorescence), obtained at 40x (Fig 7A) and 63x (Fig 7B), with 100 and 25 μm of scale bars, respectively. At Figs 7A1 and 7B1, it may be noticed a light pattern of micropermeability within the dentinal tubules (arrow) and the adhesive layer (pointers). A limited porosity and brief nanoleakage signal from the hybrid layer (asterisk) located within the B-labeled adhesive layer infiltrated throughout the intertubular dentin is shown (Fig 7B1). In the CLSM image captured in fluorescence mode, it is possible to observe an adhesive layer characterized by the presence of cylindrical long resin tags (rt) when imaged in Rhodamine excitation/emission mode (Fig 7B2) underneath the adhesive layer and a discrete dye sorption throughout its thickness when imaged in fluorescein excitation/emission mode at big magnification (Fig 7B3). A moderate reflective signal inside the dentinal tubules (Fig 7B4) (arrow) indicates the presence of some mineral components. a, adhesive layer; d, dentin; hc, hybrid complex; rc, resin composite; rt, resin tags.

Figure 8. The interfacial characterization and micropermeability of the resin-dentin interface created using the experimental adhesive applied on phosphoric acid-etched dentin

and then load cycled is shown at CLSM images (reflexion/fluorescence), obtained at 40x (Fig 8A), 63x (Fig 8B), and 63x-2 optical zoom (Fig 8C), with 100, 25 and 10 µm of scale bars, respectively. At Figs 8B1 and 8C1, a light pattern of micropermeability (arrow) within the dentinal tubules (Fig 8B3) and the adhesive layer (8C3), and between the adhesive layer and the resin composite (Fig 8C1) may be observed. A limited porosity and brief nanoleakage signal from the hybrid layer (asterisk) located within the labeled adhesive layer infiltrated throughout the intertubular dentin is shown. At the CLSM image captured in fluorescence mode, it is possible to observe an adhesive layer characterized by the presence of middle-sized funnel-shaped resin tags (rt) when imaged in Rhodamine excitation/emission mode (Figs 8C1,8C2) underneath the adhesive layer and a discrete dye sorption throughout its thickness when imaged in fluorescein excitation/emission mode (Fig 8C3). A moderate reflective signal inside the dentinal tubules (Figs 8A4, 8B4) (arrow) indicates the presence of some mineral components. a, adhesive layer; d, dentin; rc, resin composite; rt, resin tags; t, dentinal tubules.

Figure 9. CLSM single-projection images disclosing the fluorescent calcium-chelators dye xylenol orange. It is shown the interfacial characterization of the resin-dentin interface created using Futurabond U adhesive applied on smear layer-covered dentin (Fig 9A), and obtained at 63x, with 10µm of scale bar, imaged in Rhodamine excitation/emission mode (Fig 9B) and calcium-chelators dye xylenol orange only (Fig 9C). Signals of xylenol orange stain were observed at the resin dentin interface, affecting both the hybrid complex (hc) and some dentinal tubules (Figs 9A, 9C) (arrows). When imaged in Rhodamine excitation/emission mode, long resin tags were discernible (Fig 9B) underneath the adhesive layer and hybrid complex (pointer). hc, hybrid complex.

Figure 10. CLSM single-projection images disclosing the fluorescent calcium-chelators dye xylenol orange. It is shown the interfacial characterization, after load cycling, of the resin-dentin interface created using Futurabond U adhesive applied on smear layer-covered dentin, and obtained at 63x, with 10μm of scale bar, imaged in Rhodamine excitation/emission mode (Fig 10B) and calcium-chelators dye xylenol orange only (Fig 10C). Scarce and long resin tags (arrow) (Fig 10B), below a very thin hybrid complex, were detected. Dentinal tubules appeared clearly stained with XO-dye, which showed a remarkable fluorescence signal due to consistent presence of Ca-minerals within the tubules (asterisk) and walls of dentinal tubules (pointer).

Figure 11. CLSM single-projection images disclosing the fluorescent calcium-chelators dye xylenol orange. The interfacial characterization of the resin-dentin interface created using Futurabond U adhesive applied on phosphoric acid-etched dentin, and obtained at 63x, with 10μm of scale bar, imaged in Rhodamine excitation/emission mode (Fig 11B) and calcium-chelators dye xylenol orange only (Fig 11C) is shown. The interface disclosed a clear fluorescence signal within the adhesive layer (a), hybrid complex (hc) and dentinal tubules (t). XO-dye penetrated the first 10-20 μm of resin tags. The rest of resin-tags length appeared with the typical Rhodhamine B-labeled colorant. a, adhesive layer; hc: hybrid complex; t, dentinal tubules.

Figure 12. CLSM single-projection image disclosing the fluorescent calcium-chelators dye xylenol orange of the resin-dentin interface created with Futurabond U adhesive applied on phosphoric acid-etched dentin and then load cycled, and obtained at 63(x), with 10 μm

of scale bars, imaged in Rhodamine excitation/emission mode (Fig 12B) and calcium-chelators dye xylenol orange only (Fig 12C). Mineral deposition may be visualized within the hybrid complex (hc) and along the walls of dentinal tubules (t) (arrows). Note the presence of multiple intact resin tags imaged in Rhodamine excitation/emission mode (Fig 12B). hc: hybrid complex; t, dentinal tubules.

Figure 13. CLSM single-projection images disclosing the fluorescent calcium-chelators dye xylenol orange, showing the interfacial characterization of the resin-dentin interface created using the experimental adhesive applied on smear layer-covered dentin, and obtained at 63x, with 10μm of scale bar, imaged in Rhodamine excitation/emission mode (Fig 13B) and calcium-chelators dye xylenol orange only (Fig 13C). The analysis of this interface denoted the presence of a compact hybrid complex (hc), with multiple and long resin tags (t) imaged in Rhodamine excitation/emission mode. Scarce and faint XO-dye was observed in dentin (pointer). hc: hybrid complex; rt, resin tags; t, dentinal tubules.

Figure 14. CLSM single-projection images disclosing the fluorescent calcium-chelators dye xylenol orange, showing the interfacial characterization of the resin-dentin interface created using the experimental adhesive applied on smear layer-covered dentin and then load cycled, and obtained at 63x, with 10μm of scale bar, imaged in Rhodamine excitation/emission mode (Fig 14B) and calcium-chelators dye xylenol orange only (Fig 14C). The adhesive layer is characterized by the presence of prominent and discontinuous resin tags, when imaged in Rhodamine excitation/emission mode (Figs 14A, 14B). Moderate fluorescence signal of XO-dye within a wide hybrid complex (hc), but strong

within some dentinal tubules (t), revealed the presence of calcium complexes within both adhesive structures. hc: hybrid complex; rt, resin tags.

Figure 15. CLSM single-projection images disclosing the fluorescent calcium-chelators dye xylenol orange, showing the interfacial characterization of the resin-dentin interface created using the experimental adhesive applied on phosphoric acid-etched dentin, and obtained at 63x, with 10μm of scale bar, imaged in Rhodamine excitation/emission mode (Fig 15B) and calcium-chelators dye xylenol orange only (Fig 15C). Adequate penetration of the experimental adhesive into the phosphoric acid-treated dentin surface and tubules was observed. Short and robust resin tags (rt) stained with xylenol orange evidenced the sealing of the resin-dentin interface. Some empty dentinal tubules (t) appeared below the XO-dye resin tags, though with Rhodamine B infiltrating the intertubular dentin (pointer). rt, resin tags.

Figure 16. CLSM single-projection image disclosing the fluorescent calcium-chelators dye xylenol orange of the resin-dentin interface created with the experimental adhesive applied on phosphoric acid-etched dentin and then load cycled, and obtained at 63(x), with 10 μm of scale bar, imaged in Rhodamine excitation/emission mode (Fig 16B) and calcium-chelators dye xylenol orange only (Fig 16C). A clear fluorescence signal due to consistent presence of xylenol-stained Ca-deposits within the hybrid complex (hc), walls of dentinal tubules (dt) and resin tags (rt). hc: hybrid complex; rt, resin tags; t, dentinal tubules.

Figure 1 165x262mm (300 x 300 DPI)

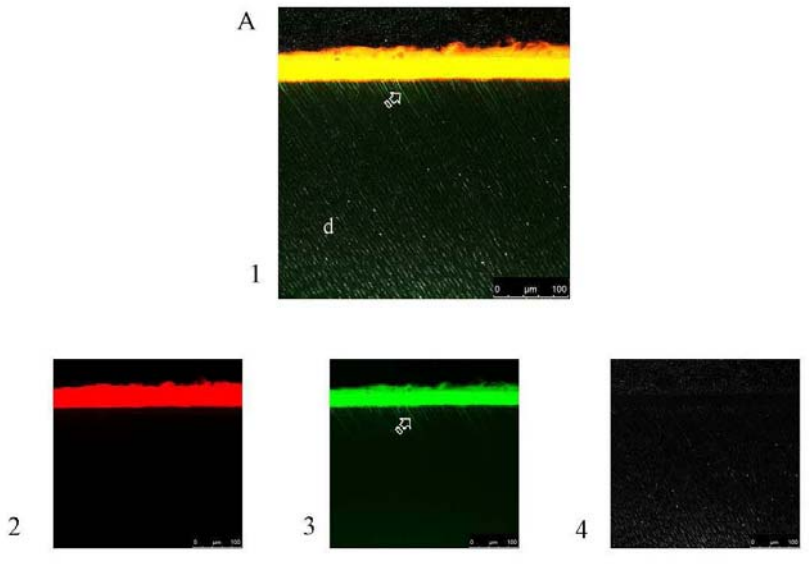

Figure 2A 181x125mm (300 x 300 DPI)

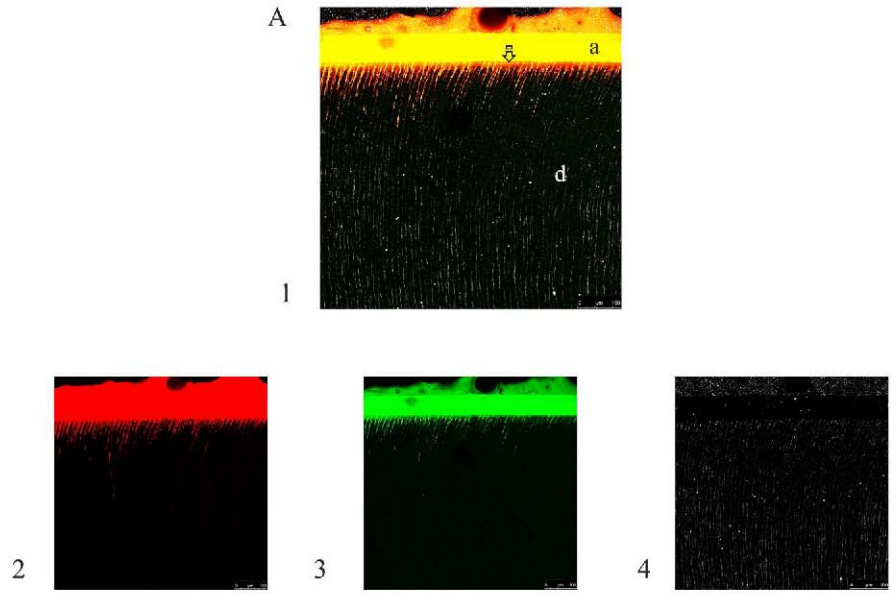

Figure 2B, 2C 167x270mm (300 x 300 DPI)

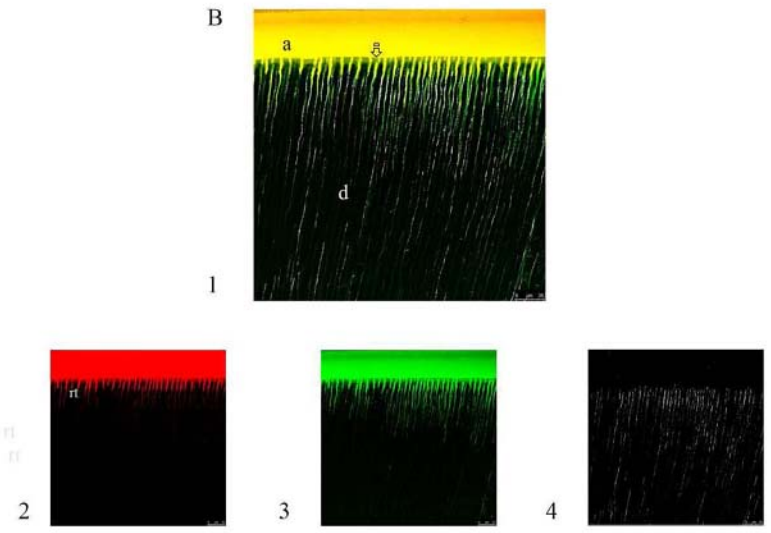

Figure 3 170x267mm (300 x 300 DPI)

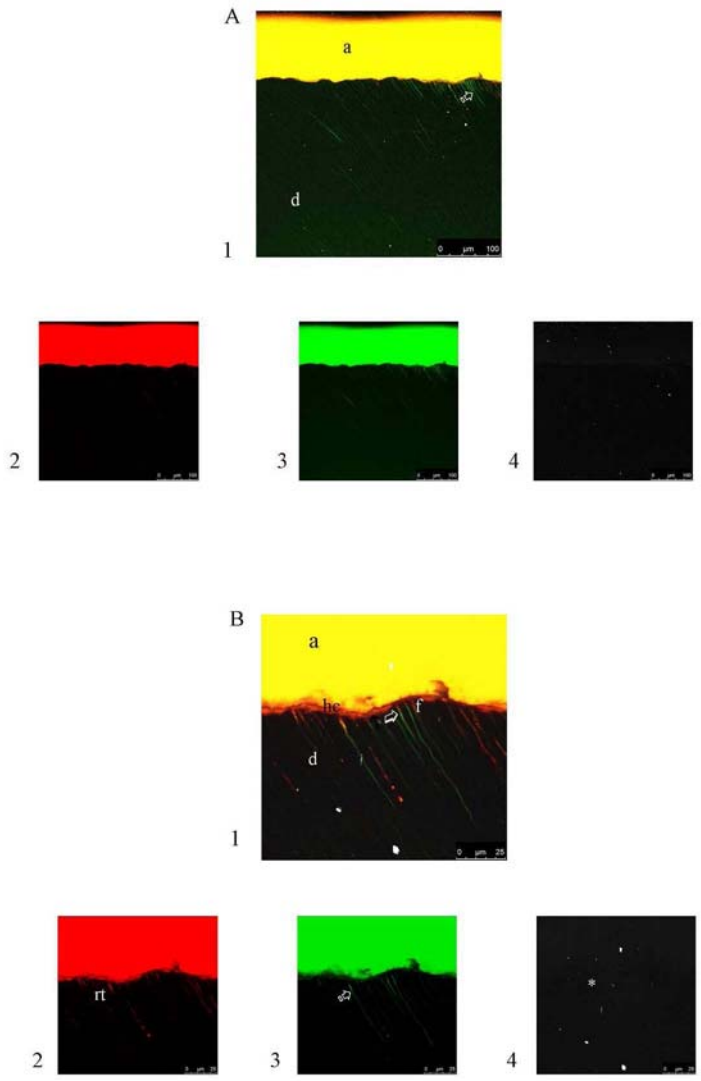

Figure 4A, 4B 170x270mm (300 x 300 DPI)

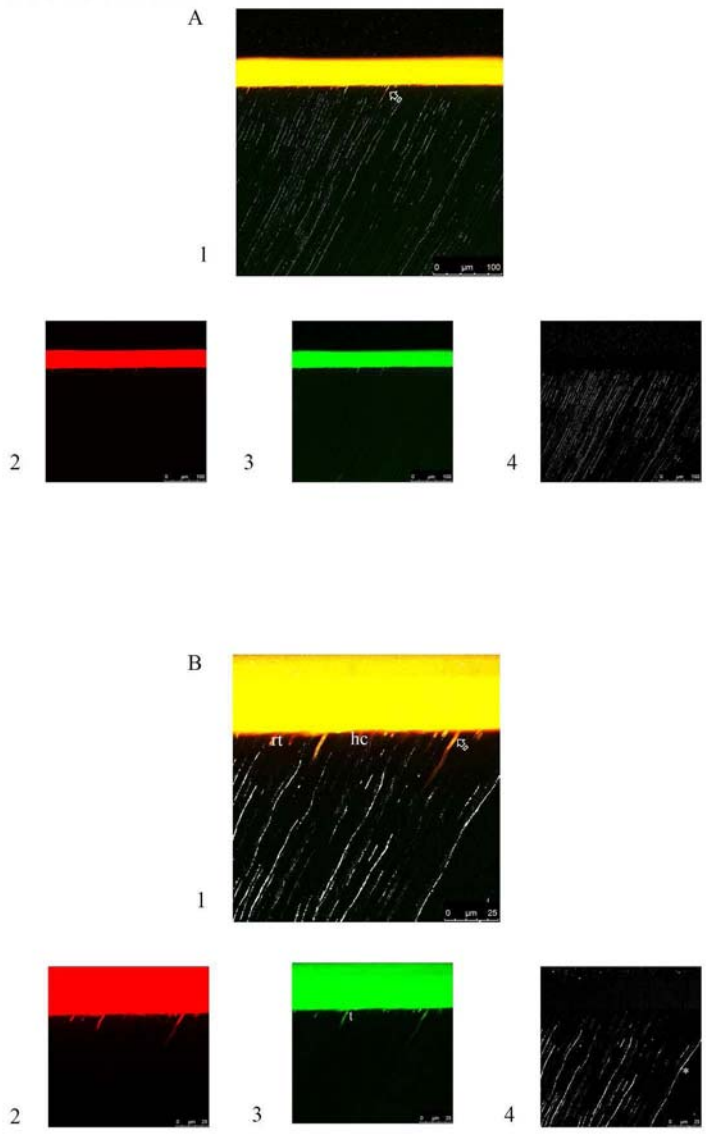

Figure 4C 170x119mm (300 x 300 DPI)

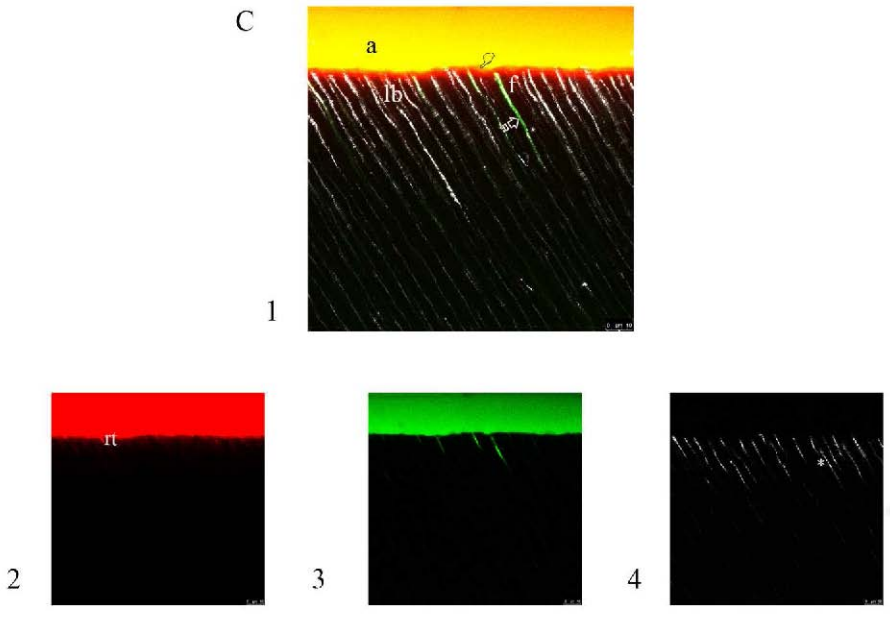

Figure 5 160x267mm (300 x 300 DPI)

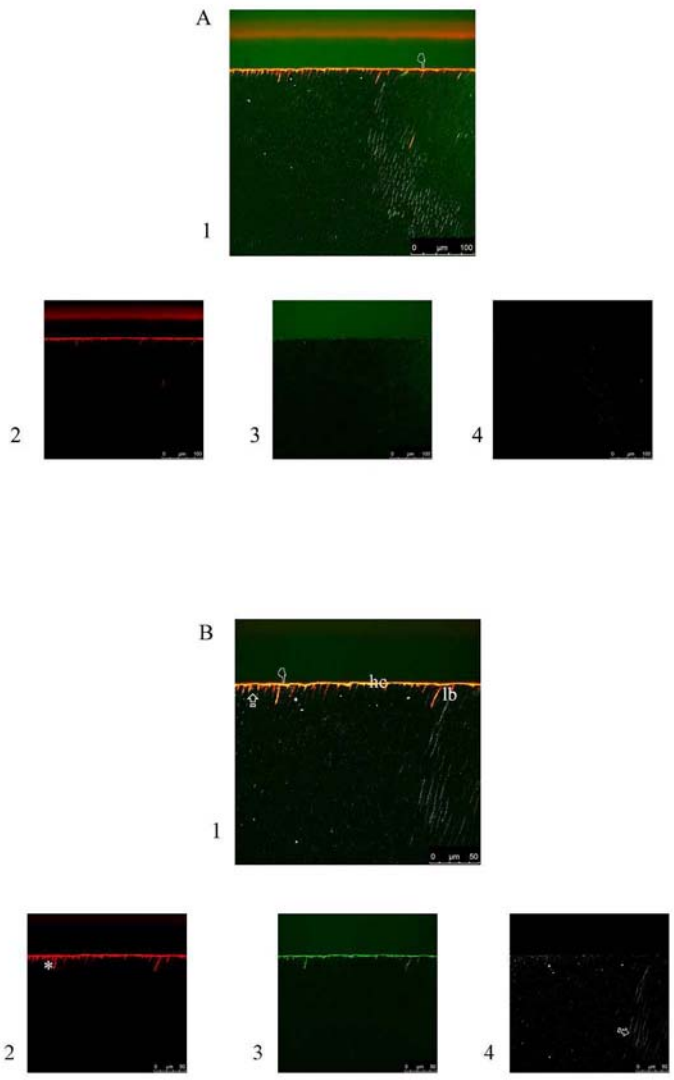

Figure 6A, 6B 170x270mm (300 x 300 DPI)

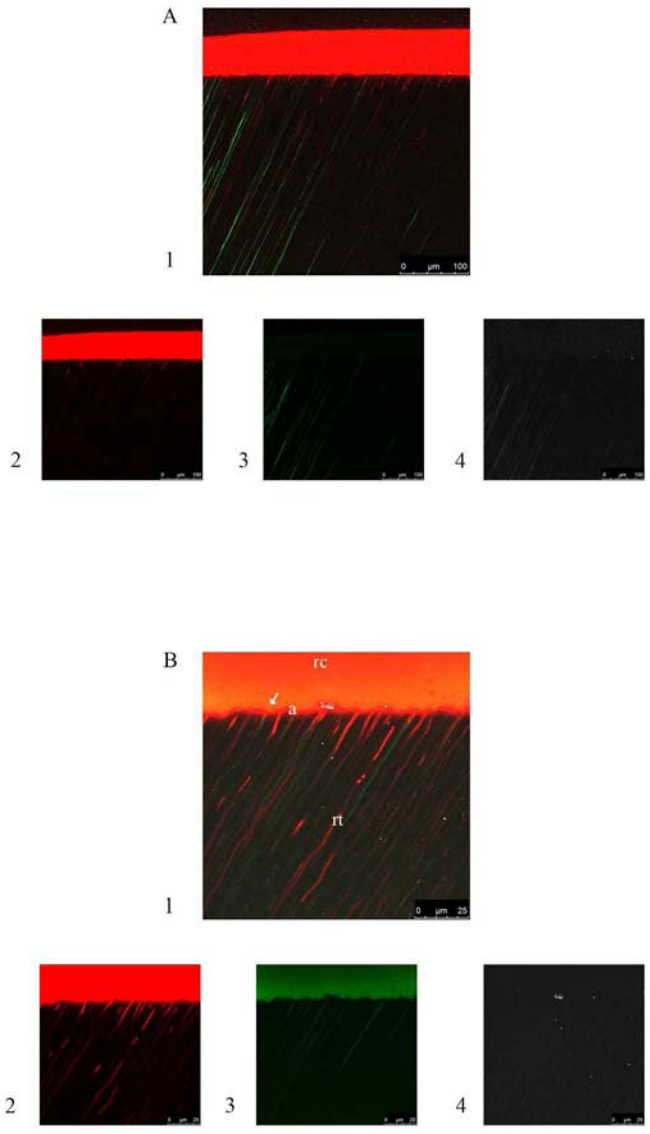

Figure 6C 170x127mm (300 x 300 DPI)

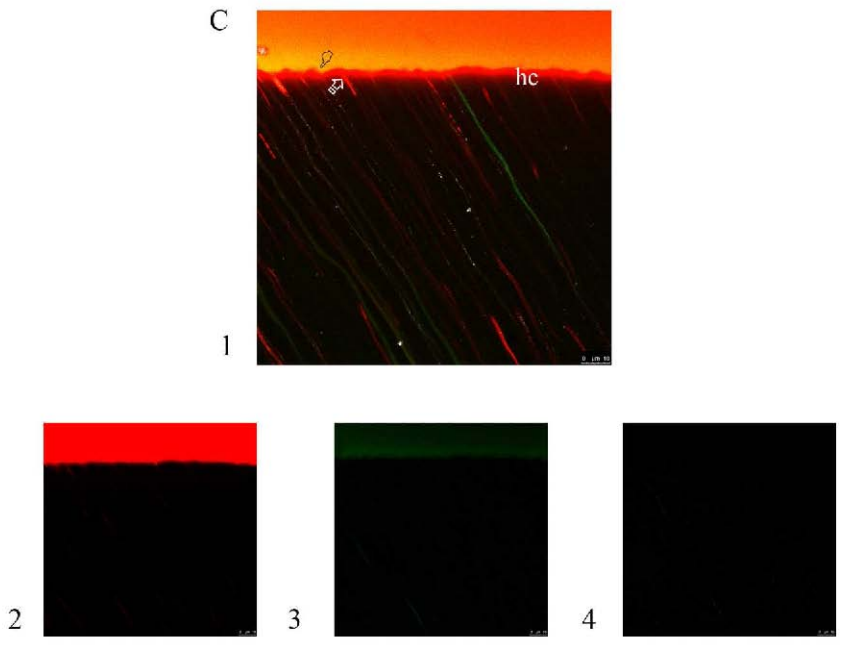

Figure 7 170x267mm (300 x 300 DPI)

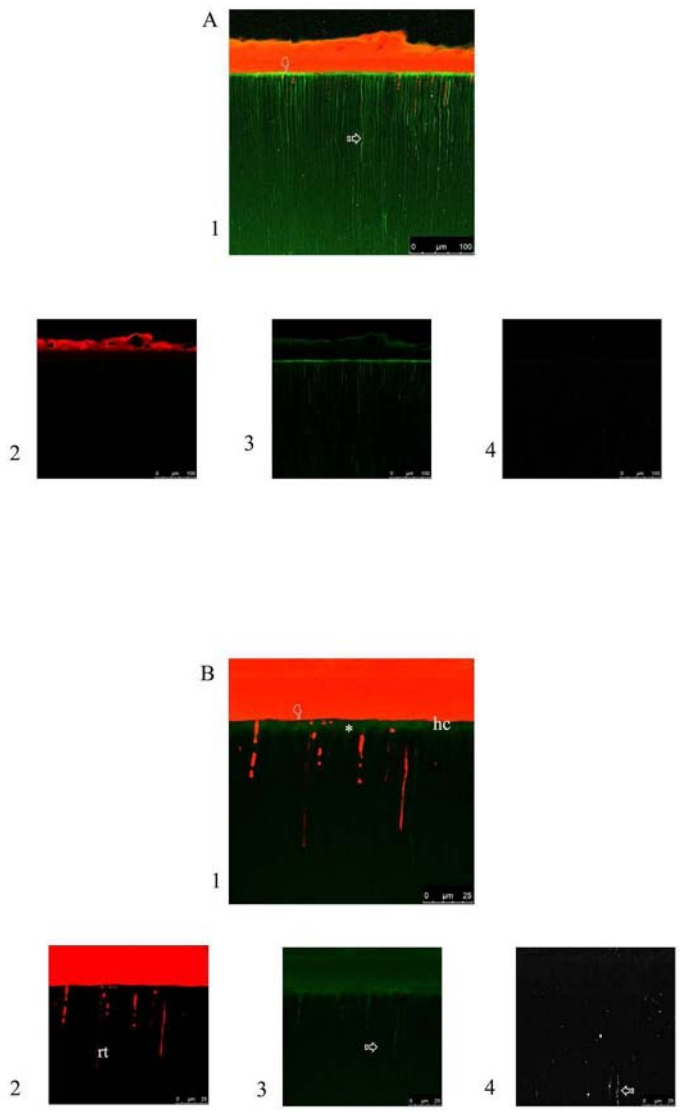

Figure 8A, 8B 162x279mm (300 x 300 DPI)

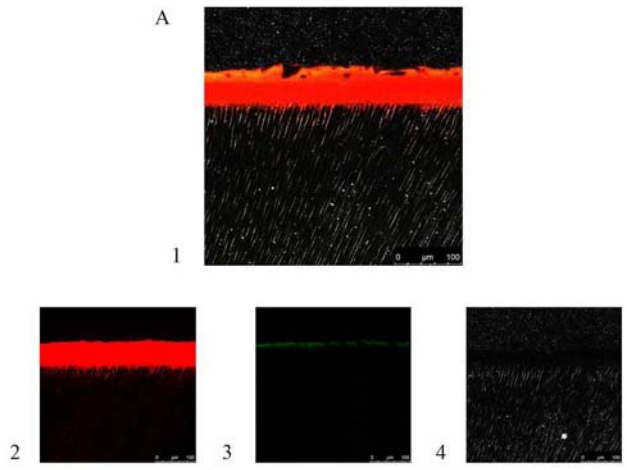

Figure 8C 157x127mm (300 x 300 DPI)

Figure 9 137x125mm (300 x 300 DPI)

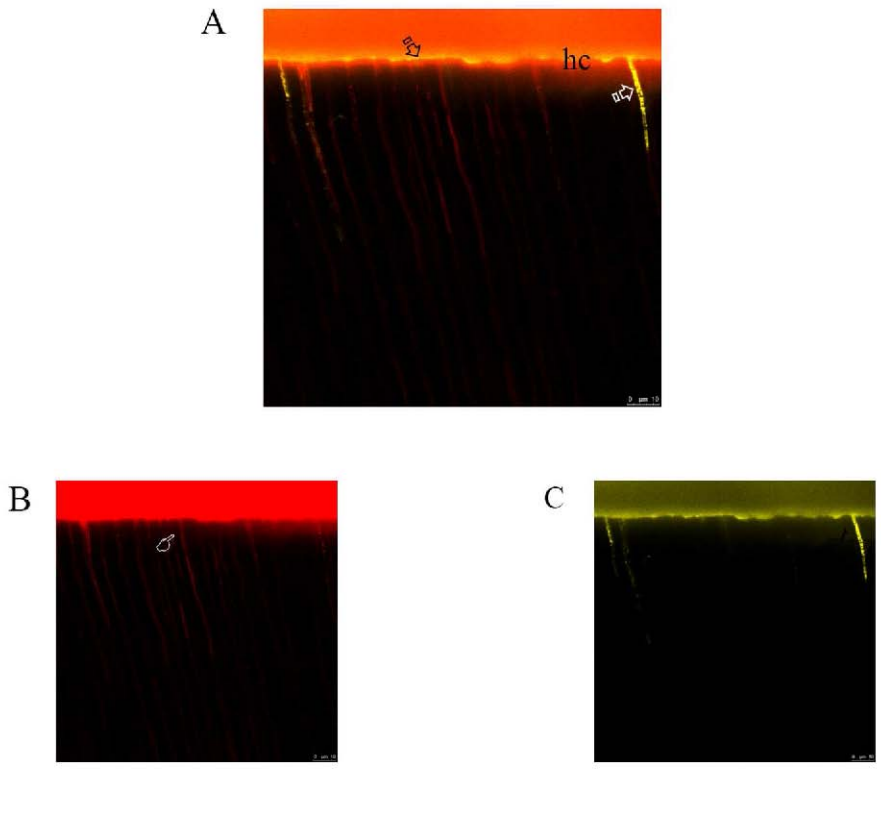

Figure 11 140x125mm (300 x 300 DPI)

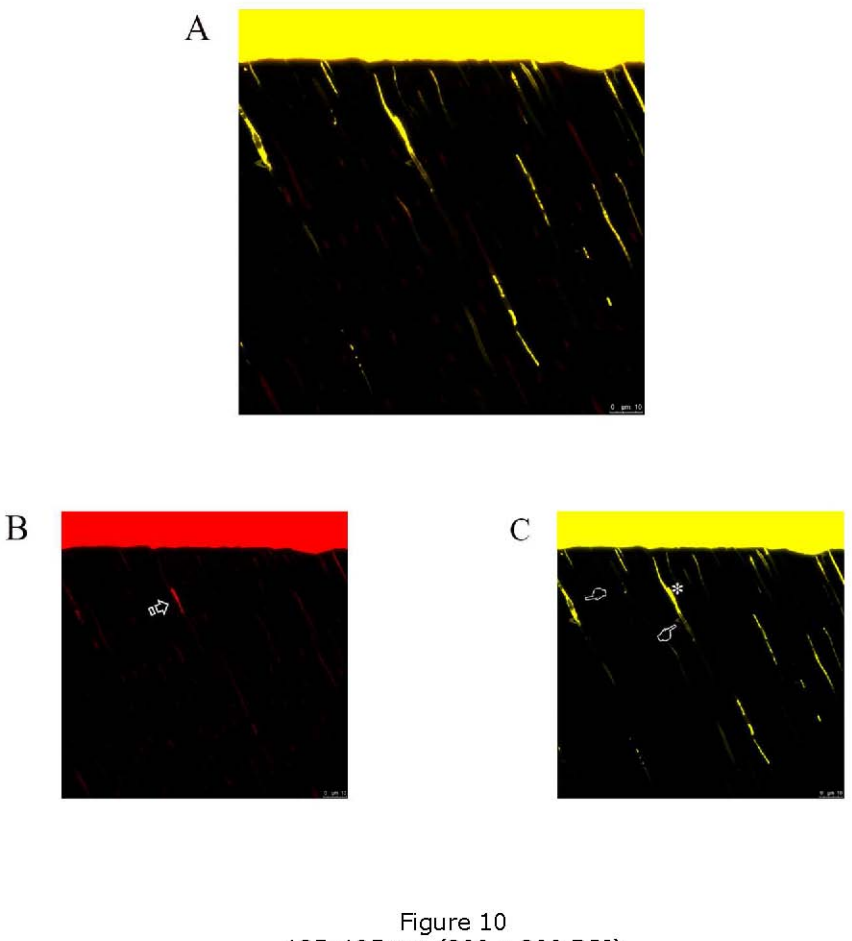

Figure 10
135x125mm (300 x 300 DPI)

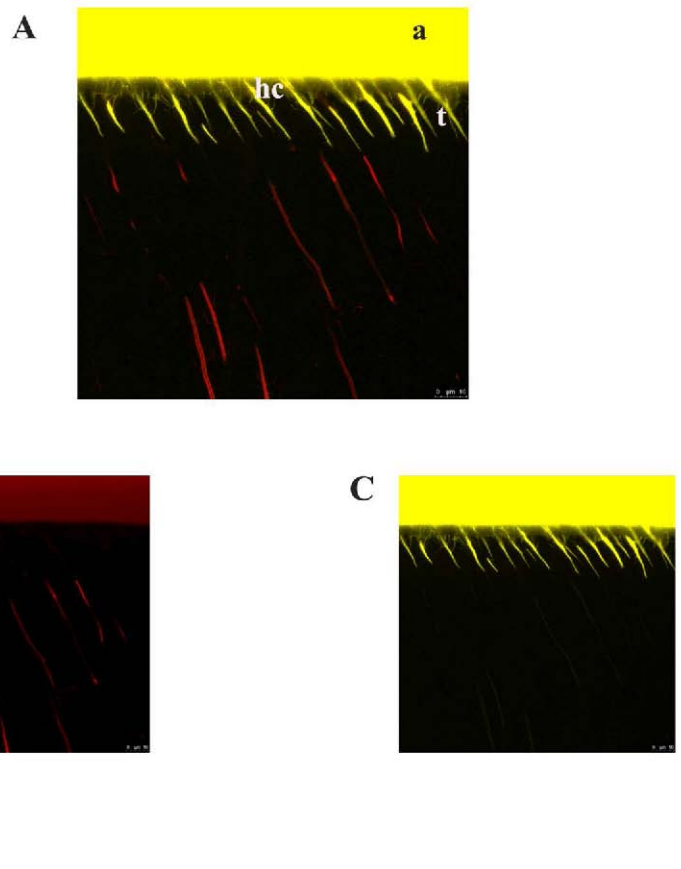

Figure 11
140x125mm (300 x 300 DPI)

Figure 12 135x125mm (300 x 300 DPI)

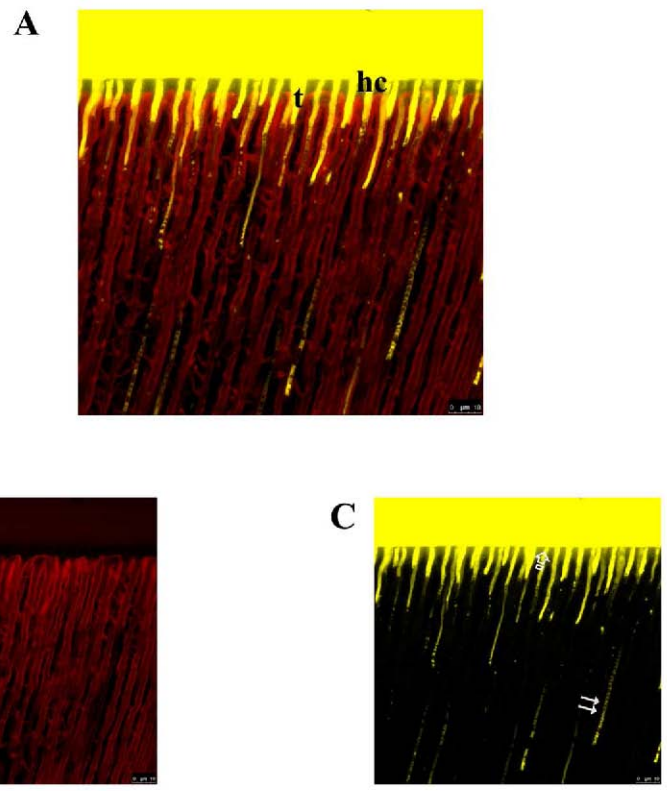

Figure 12
135x125mm (300 x 300 DPI)
Figure 13 130x125mm (300 x 300 DPI)

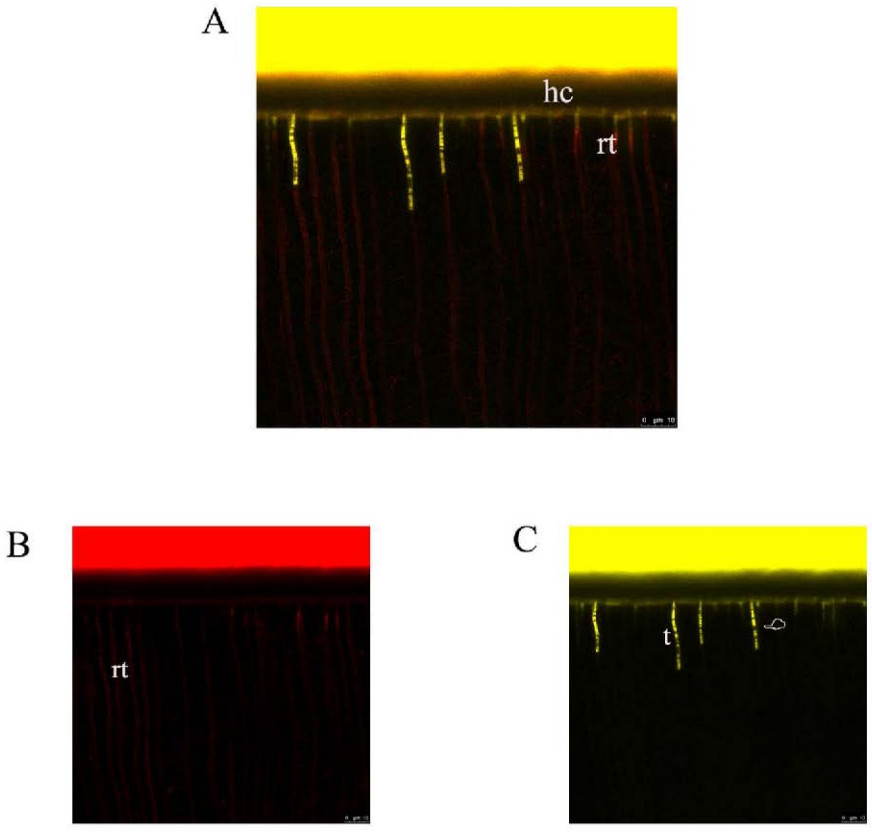

Figure 13
130x125mm (300 x 300 DPI)

Figure 14 140x125mm (300 x 300 DPI)

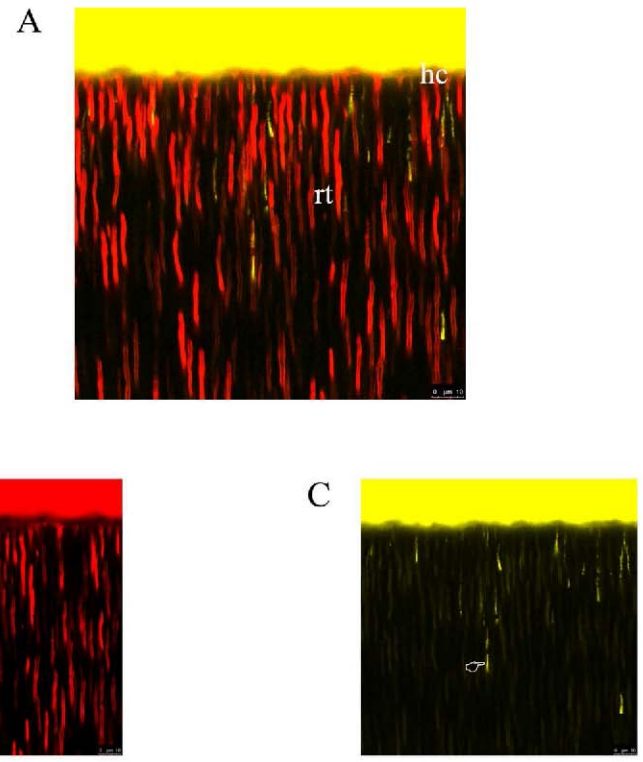

Figure 14
140x125mm (300 x 300 DPI)
Figure 15 130x125mm (300 x 300 DPI)

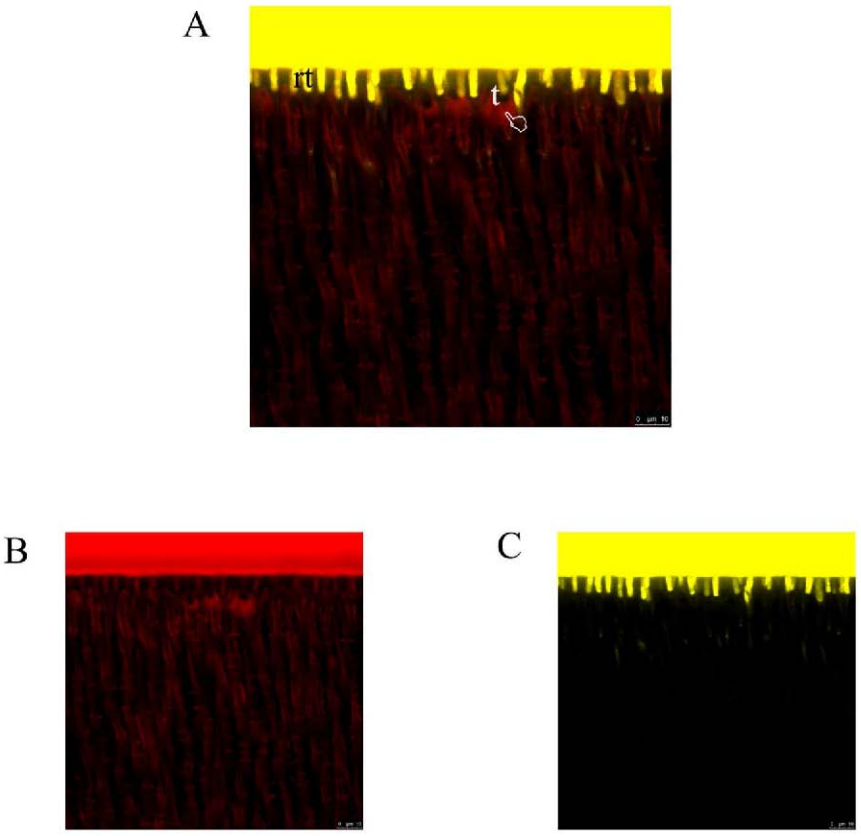

Figure 15
130x125mm (300 x 300 DPI)

Figure 16 135x125mm (300 x 300 DPI)

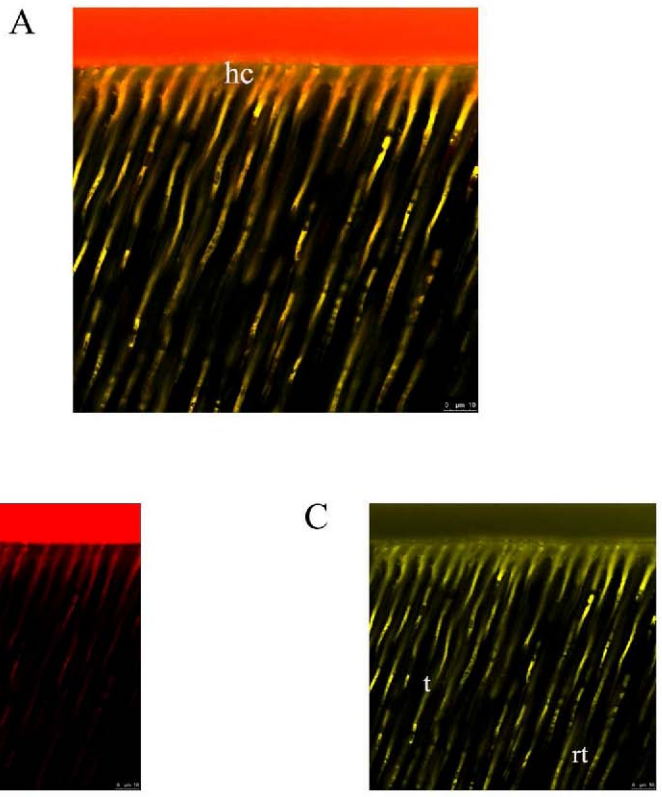

Figure 16
135x125mm (300 x 300 DPI)

Table 1. Materials and chemicals used in this study and respective manufacturers, basic formulation and mode of application.

Abbreviations: HEMA: 2hydroxyethyl methacrylate; BisGMA: bisphenol A diglycidyl methacrylate; HEDMA:

8.R2 _

8.R2 _

8.R2 _

8.R2 _

8.R2 _

8.R2 _

8.R2 _

8.R2 _

8.R2 _

8.R2 _

hydroxyethyldimethacrylate; UDMA: urethane dimethacrylate: H_3PO_4: phosphoric acid; BisEMA: ethoxylated bisphenol A glycol dimethacrylate; TEGDMA: triethylene glycol dimethacrylate;

SBFS: simulated body fluid solution; NaCl: sodium chloride; $NaHCO_3$: sodium bicarbonate; KCl: potassium chloride; $K_2HPO_4 \cdot 3H_2O$: potassium phosphate dibasic trihydrate; $MgCl_2 \cdot 6H_2O$: magnesium chloride hexahydrate; HCl: hydrogen

chloride; $CaCl_2$: Calcium chloride; Na_2SO_4: sodium sulfate; Tris: tris(hydroxylmethyl) aminomethane.

____قمح_عمي_نجح_لجم_Ô_Ʒ_K_T_ч_□_Q_W_ù_____豈_____÷_____□_____

9 Futurabond U	**10** Futurabond U	
	11 Futurabond U	
	12 Futurabond U	
	13 Experimental	
	14 Experimental	
	15 Experimental	
	16 Experimental	
no PAetch, no loadcycling	no PAetch, loadcycling	
	PAetch, no loadcycling	
	PAetch, loadcycling	
	no PAetch, no loadcycling	
	no PAetch, loadcycling	
	PAetch, no loadcycling	
	PAetch, loadcycling	
	Rd/Xo	Rd/Xo
	Rd/Xo	
	Rd/Xo	
	Rd/Xo	
	Rd/Xo	
	Rd/Xo	
	Rd/Xo	

Abreviations: PA: Phosphoric Acid; Rd: Rhodamine B; Fl: fluorescein; Xo: Xylenol orange

蠱椀最甄嫩攀. …… .. …..

…… …… .. …..

....

....

....

....

....